

Exoskeletal strength and cuticle composite profile of the acorn weevil rostrum

M. Andrew Jansen,^{1,*} Jason Williams,² Nikhilesh Chawla,² and Nico M. Franz¹

¹School of Life Sciences, Arizona State University, Tempe, AZ 85287, USA

²School for Engineering of Matter, Energy, and Transport,
Arizona State University, Tempe, AZ 85287, USA

(Dated: May 3, 2019)

The acorn weevil (*Curculio* Linnaeus, 1758) rostrum (snout) exhibits remarkable flexibility and toughness derived from the microarchitecture of its exoskeleton. Here we characterize modifications to the composite profile of the rostral cuticle that simultaneously enhance the flexibility and toughness of the distal portion of the snout. Using Classical Laminate Plate Theory, we estimate the effect of these modifications on the elastic behavior of the exoskeleton. We show that the tensile behavior of the rostrum across six *Curculio* species with high morphological variation correlates with changes in the relative layer thicknesses and orientation angles of layers in the exoskeleton. Accordingly, increased endocuticle thickness is strongly correlated with increased tensile strength. Rostrum stiffness is shown to be inversely correlated with work of fracture; thus allowing a highly curved rostrum to completely straighten without structural damage. Finally, we identify exocuticle rich invaginations of the occipital sutures both as a likely site of crack initiation in tensile failure, and as a source of morphological constraint on the evolution of the rostrum in *Curculio* weevils.

The exoskeleton of Coleoptera (beetles) is a hierarchically structured, fibrous composite – characterized by variously arranged α -chitin (N-acetylglucosamine) nanofibrils that are embedded in a heterogeneous protein matrix [1–3]. Although α -chitin is brittle and strongly anisotropic, beetle cuticle is simultaneously rigid and tough due to its unique laminate microstructure (reviewed in [4–6]), characterized in detail below. Impact-prone areas and exaggerated structures in arthropods generally exhibit cuticle organization that resists deformation and fracture [7–11]. However, acorn weevils in the genus *Curculio* Linnaeus, 1758¹ (Curculionidae in the sense of [13]) instead exhibit unusual distal flexibility in an elongate extension of the head called the rostrum (snout) [1, 14–16]. The rostrum is a hollow, strongly curved (over 90° in some species), cylindrical, exoskeletal extension of the otherwise nearly-spherical head, which bears at its apex the terminal chewing mouthparts [16–20]. This structure is used by the female to feed on fruit (plant) tissue and to excavate sites for egg-laying (oviposition, see Fig. 1). The rostrum can be repeatedly bent, without evident damage, and despite being composed of the same material as other rigid body parts [1, 14–16]. By maintaining constant pressure on the snout and rotating around the bore-hole, females are able to flex the rostrum into a straightened configuration and produce a linear channel into the fruit. A single adult female may prepare hundreds of such sites [15, 21, 22].

Despite its documented performance in many *Curculio*

species [15, 16, 21, 22], it remains unknown how the rostrum of female acorn weevils can withstand the repeated, often extreme bending incurred during the process of egg-chamber excavation. In this study, we therefore characterize the composite profile of the rostral cuticle to account for the observed flexibility of the snout. We show that the relative layer thicknesses and fiber orientation angles of the exocuticle and endocuticle of the rostrum are strongly differentiated from the head capsule and other body parts. The effect of these differences on the elasticity of the cuticle is estimated using Classical Laminate Plate Theory (CLPT). Recent studies have shown that the yield strength of the beetle exoskeleton is lower in tension than compression [23]. To assess the validity of these findings, we compare the ultimate tensile strength of the rostrum across species and snout morphotypes. We also report displacement-controlled load cycling results for the snout of one *Curculio* species with strongly curved morphology. Our results indicate that an increase in the volume fraction of endocuticle in the rostrum conveys higher tensile strength at the rostral apex across all tested species; and further, that a strongly curved rostrum can be flexed repeatedly without harm to the structure.

* corresponding author, email: majanse1@asu.edu

¹Pursuant to the International Code of Zoological Nomenclature, the first mention of any specific epithet will include the full genus and species names as a binomen (two-part name) followed by the author and date of publication of the name. This is not an in-line reference; it is a part of the name itself and refers to a particular act establishing the validity and fixing the identity of the corresponding name by that author [12].

We additionally describe the fracture mechanics of the snout, while considering how modification of the cuticle may prevent crack formation during oviposition. Accordingly, the flexibility and tensile strength of the rostrum appear to be derived exclusively from modification of the composite architecture of the exoskeleton. This is the first time that a modified composite profile has been reported as a means of enhancing structural elasticity in the insect exoskeleton (though see [24]).

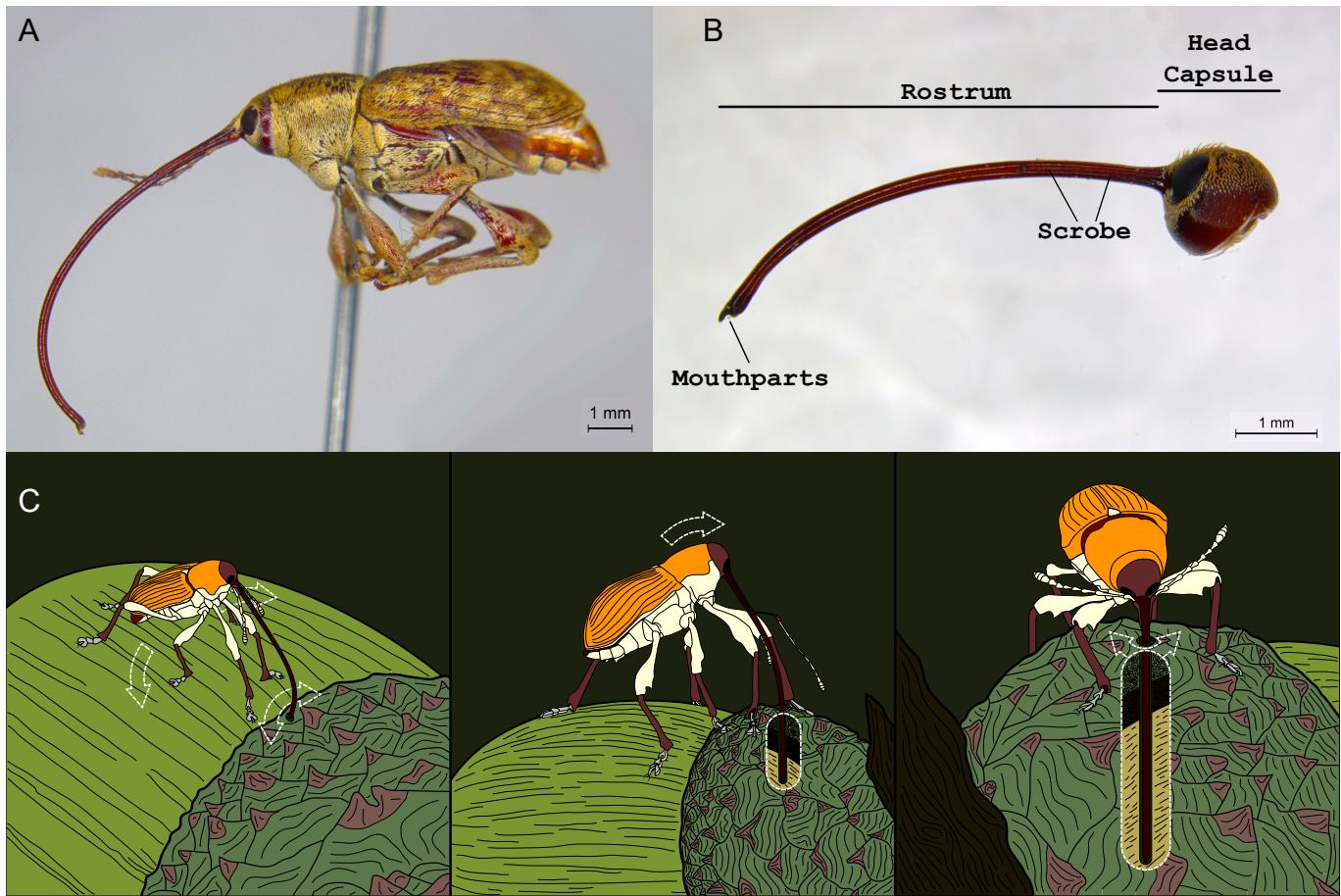


FIG. 1. Morphology and oviposition behavior of female *Curculio* weevils. a, Lateral habitus image of female *Curculio sayi* (Gyllenhal, 1836) featuring the elongate, strongly curved rostrum. b, Lateral view of head of female specimen of *Curculio longinasus* Chittenden, 1927, with major anatomical features indicated. c, Illustration of oviposition behavior, proceeding from left to right: female makes incision in host fruit, flexes head directly over bore-hole using front legs, then maintains tension on snout while rotating to excavate linear channel into fruit. During this process, female rostrum is bent until completely straight.

68 I. MICROSTRUCTURE OF THE CURCULIO 69 ROSTRUM

70 In arthropods – including beetles – the exocuticle is
71 comprised of numerous unidirectional laminae of chitin
72 nanofibrils. Each layer is the thickness of a single fiber
73 (2-4 nm) embedded in a proteinaceous matrix [25, 26].
74 These layers are stacked at a more or less constant angle
75 to each other, forming a quasi-isotropic laminate known
76 as the Bouligand structure [6, 27, 28]. This layout effec-
77 tively mitigates the strong anisotropy of α -chitin, thus
78 yielding a versatile building material for the exoskeleton
79 [2, 25, 26, 29]. Beetle endocuticle, however, is unique
80 among arthropods and is comprised of large – 1-5 μm
81 diameter in *Curculio* – unidirectional bundles of chitin,
82 called macrofibers. Chitin macrofibers are orthotropic (ax-
83 ial: $E_1 = 8.5 \text{ GPa}$; transverse: $E_2 = E_3 = 0.52 \text{ GPa}$
84 [1]), and arranged in unidirectional plies, as depicted in
85 Figs. 2, 3 [4, 5]. Typically, adjacent macrofiber laminae
86 are paired and pseudo-orthogonal – i.e., angled nearly 90°

87 to each other (see Fig. 3; [30]) – with a constant stacking
88 angle between pairs, although other configurations have
89 been observed [3–5, 31]. This geometric sequence of the
90 macrofiber laminae yields an approximately transversely
91 isotropic composite, similar to the Bouligand structure
92 [5, 26]. Notably, the resulting laminate is less rigid than
93 the exocuticle, but exhibits greater toughness because the
94 pseudo-orthogonal plies effectively inhibit crack formation
95 and propagation between successive layers [3–5].

96 Serial thin sectioning and scanning electron microscopy
97 of fractured *Curculio* specimens reveals that endocuti-
98 cle in the head capsule fits this general profile, with an
99 angle of nearly 30° between successive pairs of pseudo-
100 orthogonal plies. Additionally, in the head capsule, the
101 thickness of the exocuticle and endocuticle in cross-section
102 is nearly equal – typically between 20-30 μm . However,
103 the cuticle composite lay-up of the rostral apex is strongly
104 differentiated from the head capsule, as shown in Fig. 3.
105 Distally the exocuticle is reduced to a thin shell (ca. 5
106 μm), with the endocuticle thickened to offset this reduc-

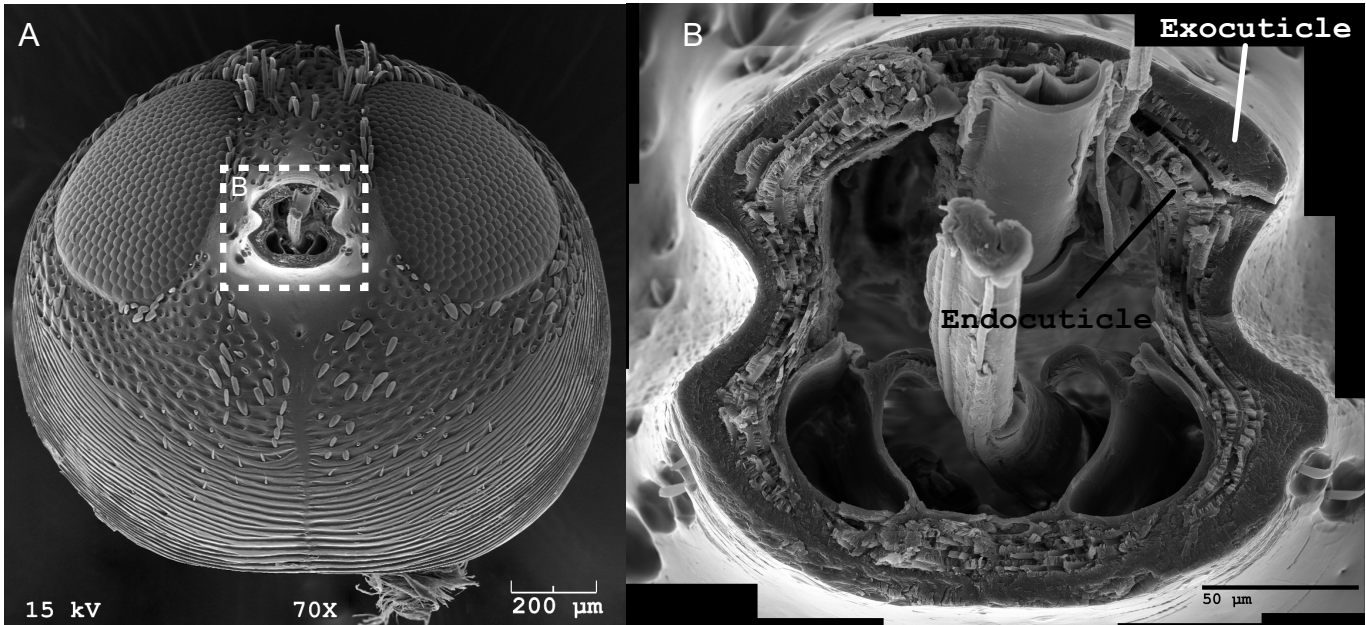


FIG. 2. Gross divisions of cuticle in the female *Curculio* rostrum. **a**, Scanning electron micrograph of head capsule, in frontal view, of female *Curculio sulcatus* (Casey, 1897), with rostrum removed. **b**, Magnified view of junction between rostrum and head capsule, showing division of cuticle into two general regions: exocuticle and endocuticle.

tion and maintain a constant cuticle thickness (ca. 50 μm total) throughout its length. Moreover, the endocuticular macrofibers exhibit no rotation between successive pseudo-orthogonal plies; and are oriented at approximately $\pm 45^\circ$ to the longitudinal axis of the snout (i.e., an antisymmetric $[\pm 45^\circ]$ angle-ply laminate). We previously identified these modifications to the composite structure of the cuticle within a single species, *Curculio longinasus* Chittenden, 1927 [1, 14]. However, this composite profile is herein reported in the rostrum of six additional, phylogenetically disjoint, species, suggesting that this is an evolutionarily conserved trait throughout the genus *Curculio*. In all examined species, the portion of the snout between the head capsule and apex of the scrobe exhibits a gradual transition in composite profile along an anterior-posterior gradient.

Here we estimate the effect of differential cuticle organization on uni-axial membrane and on transverse-flexural Young's moduli of the cuticle in the rostral apex and head capsule using CLPT [32, 33]. The effective elastic constants of the cuticle regions of *Curculio longinasus* – estimated previously [1] – are used to construct constitutive equations for the entire cuticle of that species. The cuticle of the head capsule is estimated to have membrane and flexural moduli of $E_m = 4.77 \text{ GPa}$ and $E_f = 6.04 \text{ GPa}$, respectively. In the rostral apex these values are reduced by approximately 72% and 60%, respectively ($E_m = 1.36 \text{ GPa}$; $E_f = 2.44 \text{ GPa}$). Two hypothetical cuticle lay-ups are also modeled to individually assess the contributions of either modified layer thickness or stacking angle sequence to the cuticle's flexibility. The effective moduli of a configuration with the angle stacking

sequence of an otherwise typical cuticle (i.e., in the head capsule) that shows layer thicknesses of the rostral apex are calculated as $E_m = 3.73 \text{ GPa}$, $E_f = 4.31 \text{ GPa}$; representing 22% and 29% decreases from unmodified cuticle, respectively. Similarly, a hypothetical cuticle with the layer thicknesses of ordinary cuticle yet possessing the angle stacking sequence of the rostral apex (i.e., $\pm 45^\circ$ angle-ply in the endocuticle) has effective elastic moduli of $E_m = 3.77 \text{ GPa}$, $E_f = 5.76 \text{ GPa}$; representing 21% and 4.7% decreases from unmodified cuticle, respectively. Each of the cuticle modifications noted in the rostral apex individually decrease the elastic moduli of the cuticle. However, they appear to have a synergistic combined effect on cuticle elasticity, rather than a simple additive effect. This result suggests that both modifications are necessary in order for the snout to function properly in the living individual – where the combined effect allows the rostrum to bend until completely straight without fracture.

II. FORCE-CONTROLLED LOADING TO FRACTURE

To better characterize the failure behavior of the female rostrum, we performed tensile testing on the snouts of six *Curculio* species that representing a mixture of closely and distantly related taxa [34–37]. Each specimen was first immersed in di-H₂O for 24 hours to simulate the living tissue (see [38]), then subjected to force-controlled, uniaxial loading to fracture at a constant stress rate of 1.0 g f · s⁻¹. In general, the specimens exhibited a non-

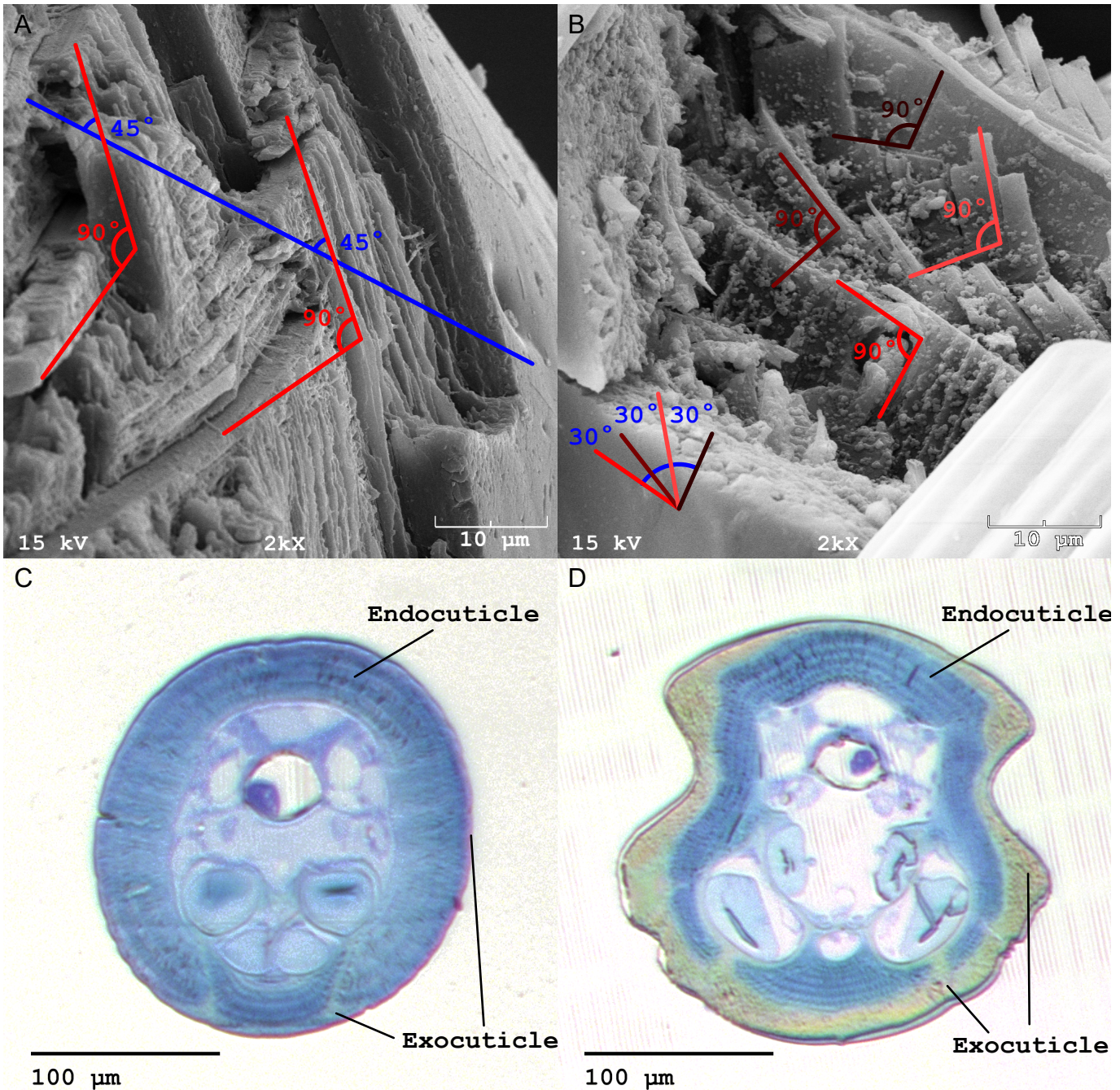


FIG. 3. Composite profiles of rostral *Curculio* cuticle. **a**, Scanning electron micrograph of fractured specimen of *Curculio humeralis* (Casey, 1897), showing that cuticle of rostral apex is organized as $\pm 45^\circ$ angle-ply laminate. **b**, Scanning electron micrograph of fractured specimen of *Curculio caryaee* (Horn, 1873), showing that cuticle of rostral base and head capsule has approximately 30° stacking angle between each pair of pseudo-orthogonal plies. **c-d**, Semi-thin sections of cuticle from specimen of *Curculio humeralis*, stained with toluidine-blue-borax; demonstrating: **(c)** that exocuticle of rostral apex is reduced to thin shell close to $5\text{ }\mu\text{m}$ thick, with endocuticle thickened to maintain a constant laminate thickness; and, **(d)** that exocuticle of head capsule and base of snout occupies nearly half of through-thickness of cuticle.

linear viscoelastic response curve characterized by a sharp increase in stress at higher strains, terminating in brittle fracture [39]. We suggest that strain hardening occurs as the longitudinal axis of the macrofibers becomes more closely aligned to the cylindrical axis of the rostrum, thereby resisting tension more directly with increasing strain [40].

We also examined the correspondence between com-

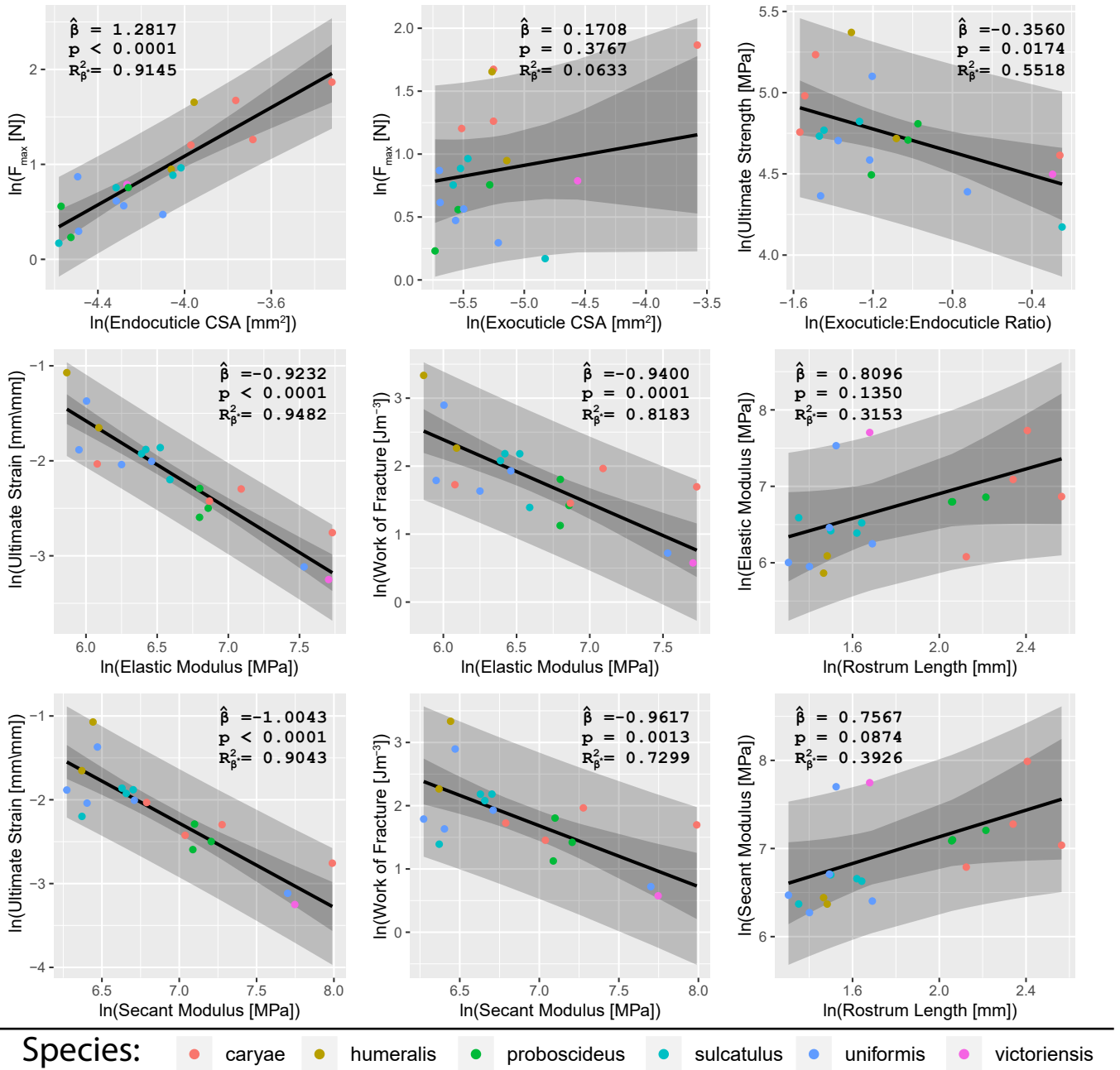


FIG. 4. Tensile properties of the female *Curculio* rostrum. Each plot shows relationship between two variables as predicted by phylogenetic linear mixed-effect model; with species as random effect and variance-covariance matrix generated from Brownian motion over preferred phylogeny of [35]. Gray regions represent the prediction interval and bootstrapped 95% confidence interval of model. The estimated fixed effect $\hat{\beta}$ is given, along with p-value of t-test assessing whether $\hat{\beta}$ is significantly different from zero. Generalized marginal $R^2_{\beta^*}$ for assessing fixed effects is also reported. In general, increased endocuticle thickness is associated with greater tensile strength, and stiffness is inversely correlated with toughness.

posit structure and mechanical behavior of the snout in an evolutionary, comparative context. Phylogenetic linear mixed effects models (PGLM, Fig. 4) were used to account for phylogenetic non-independence in residual variance, with species membership included as a random effect [41, 42]. The resulting models show that the maximum force sustained at the site of failure is strongly

correlated with the cross-sectional area of the endocuticle ($\hat{\beta} = 1.28$, $p < 0.0001$), and not the exocuticle ($\hat{\beta} = 0.17$, $p = 0.38$), at that site. There is thus a negative correlation between ultimate tensile strength of the specimen and the cross-sectional exocuticle-to-endocuticle area ratio at the fracture site ($\hat{\beta} = -0.36$, $p = 0.017$). Although CLPT predicts a positive association between

the proportion of exocuticle and stiffness of a generalized cuticle, we found no evidence of correspondence between the cross-sectional properties of the fracture site and the overall performance of the rostrum. This result is not too surprising however; because the cross-sectional areas of the cuticle regions vary across the length of the head along an anterior-posterior gradient, it is not possible to correlate measurements from the fracture surface to properties of the entire rostrum.

Instead, we found that the uniaxial elastic modulus (low strain: E_{low}) and secant modulus at failure (E_{sec}) were inversely correlated with ultimate strain and work of fracture (see Fig. 4). This implies that stiffer specimens – and by extension, stiffer cuticle profiles – are generally more brittle. We also observed a moderate, but not statistically significant, stiffening size-effect with respect to rostral length. This runs contrary to our expectation that a longer, more strongly curved rostrum would require increased flexibility to avoid fracture during oviposition [36, 37]. It is possible that longer rostra also have a longer transition gradient from basal to apical profile; thereby reinforcing the junction between the rostrum and head capsule against buckling. Young's modulus of the rostrum would be comparatively higher in such species, due to the higher volume fraction of exocuticle. We therefore posit that the gross elastic performance of the cuticle is consistent across the weevil genus *Curculio*. A single mechanism – i.e., the modified composite profile – likely confers increased flexibility and tensile strength to the rostral apex across all *Curculio* species. In addition, the endocuticle demonstrably contributes more to rostral tensile strength than the exocuticle; likely because of its organization into large bundles of aligned, anisotropic fibers, and amounting a trade-off between rigidity and toughness. Consequently, the altered composite profile of the cuticle in the rostral apex makes the rostrum simultaneously more flexible and fracture-resistant.

III. LOAD CYCLING OF THE PECAN WEEVIL

To confirm that repeated, prescribed straightening of the rostrum does not result in damage to the cuticle, we performed displacement-controlled fatigue testing on a typical female specimen of the pecan weevil *Curculio caryae* (Horn, 1873) – a species that exhibits extreme (80–90°, Fig. 5) rostral curvature [16, 21]. The specimen was aligned so that uniaxial tension would induce elongation of the distal portion of the rostrum with minimal off-axis deflection of the uncurved section. The strain per cycle was fixed at an amplitude sufficient to completely elongate the rostrum and generate a tensile load of 1.0 N in the straightened configuration (ca. 20% ultimate strength), at a frequency of 0.33 Hz. The test was terminated after a period of two weeks – i.e., ca. 400,000 cycles – when the stress amplitude appeared to reach an asymptotic minimum. The rostrum behaved viscoelastically, indicated by hysteresis in the stress-strain

relationship during each cycle. Strain amplitude decreased logarithmically with cycle number, and the specimen appeared to have been deformed plastically and permanently during the test. However, after cleaning the specimen in a 24-hour wash with ethanol and water, the rostrum had returned to its original shape (Fig. 5).

While we cannot fully determine the cause for rostrum stress relaxation *after* testing, we speculate that it arose from the general mechanism associated with cuticle viscoelasticity. The endocuticle is made of aligned α -chitin nanofibrils whose crystalline structure is enforced by hydrogen bonds between individual chitin chains and through the protein matrix along their length. Macroscopic viscoelastic behavior results from slippage between these chains in response to shearing between the chitin molecules [2, 43, 44]. Repeated strain may have caused such slippage in the endocuticle of the rostral apex during the fatigue test. Without sufficient time for the material to completely relax after deformation, the rostrum would slowly accumulate strain and deform viscoelastically [40]. After immersion in ethanol and water, however, the cuticle would be sufficiently plasticized to allow the rostrum to return to its original configuration, thus dissipating the accumulated strain.

The specimen did not show any evidence of fractures, micro-tears, or shear cusps anywhere in the surface of the exocuticle. Moreover, the tensile strength of the tested specimen's rostrum was consistent with that of other species members ($F_{max} = 5.02$ N). Surprisingly, the specimen remained undamaged by the testing. We therefore conclude that under normal life conditions, repeated bending of the rostrum does not exceed the yield strength of the cuticle.

IV. FRACTOGRAPHY OF CURCULIO TEST SPECIMENS

In light of the complex failure modes evident in the fractured specimens, it was not always possible to identify void nucleation and crack initiation sites. We observed several patterns characteristic of both the micro-scale behavior of the cuticle and the meso-scale behavior of the rostrum during uniaxial tensile failure (Fig. 6). These patterns are described below.

In transverse view, the exocuticle consistently presented a nearly continuous fracture surface. This is characteristic of comparatively brittle failure – presumably due to the relatively homogeneous arrangement of α -chitin laminae in the Bouligand structure [25, 26]. The exocuticle typically appeared to fracture at lower strains than the endocuticle, with shear-cusp formation evident both at the fracture surface and across exocuticle adjacent to the plane of fracture [45]. Conversely, the endocuticle exhibited severe delamination, off-axis ply-splitting, and fiber-pulling away from the fracture surface. This is indicative of the relatively high toughness of the unidirectional α -chitin organization within the macrofibers

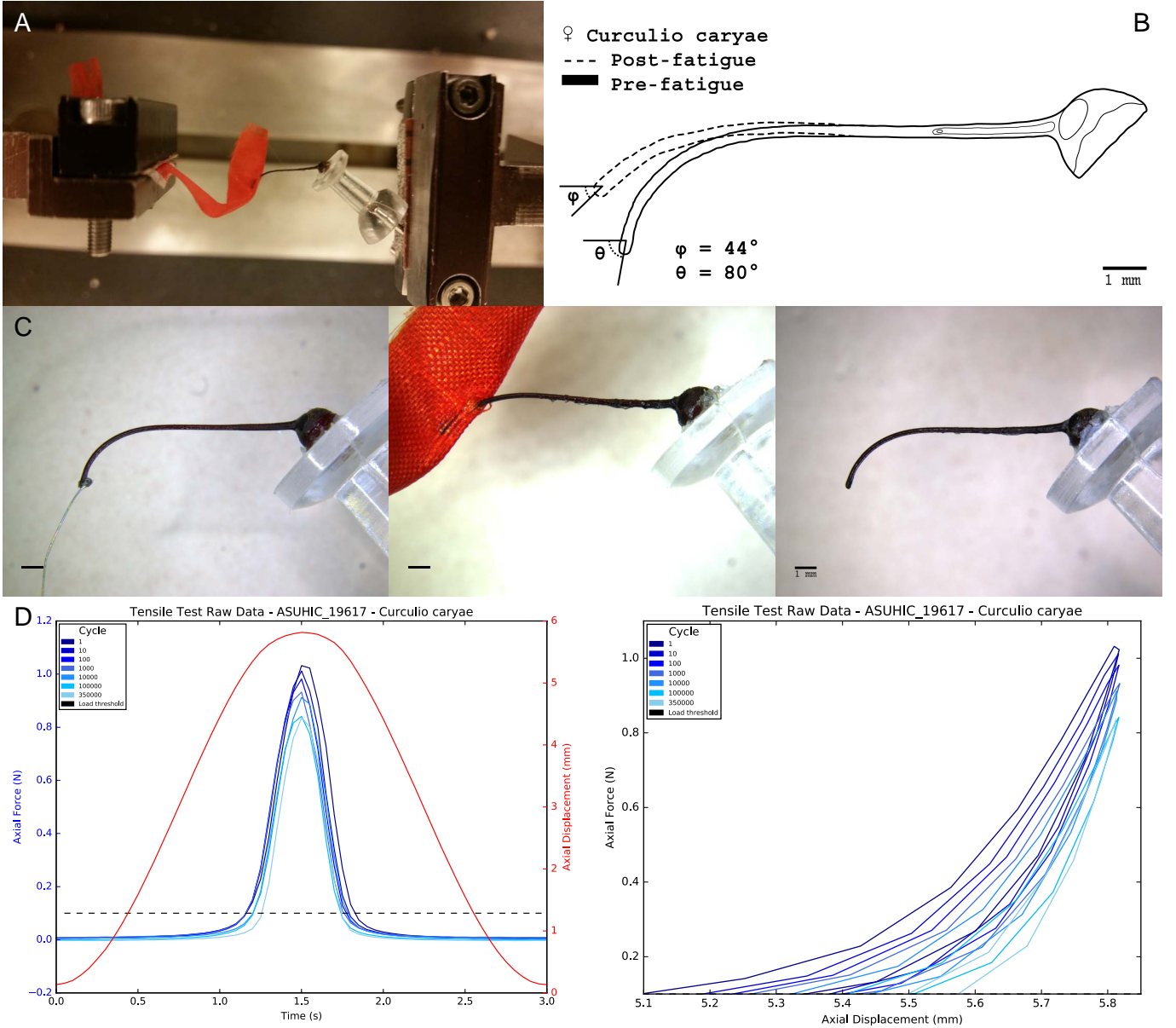


FIG. 5. Fatigue testing of a female *Curculio caryae* rostrum. **a**, Set-up of fatigue testing, with female's head capsule fixed to pedestal and rostrum attached to strip of rip-stop nylon fabric using cyanoacrylate adhesive. Specimen was loaded in tension, as opposed to compression, therefore isolating effect of tension on fatigue behavior of rostrum. **b**, Overlay of pre- and post-fatigue states of head, showing clear (short-term) effect from repeated prescribed strain. **c**, Three-photograph sequence of pre- and post-fatigue states of the rostrum; with left and central panels showing conditions immediately prior to and after testing, respectively, whereas right panel shows head having returned to its original shape after 24 hours off soaking in a water/ethanol mixture. Hence immediate post-fatigue shape is not permanent. **d**, Raw force data (left) and displacement data (right) plots for fatigue test. Displacement data plot shows clear viscoelastic behavior, indicated by hysteresis in stress-strain response of specimen, and exhibits logarithmic decrease stress amplitude over time.

300 [4, 5]. Because the exocuticle of weevils is anchored to
301 the endocuticle by cross-linking fibers (see [5, 23]), exocu-
302 ticular shear-cusp formation in uniaxial tension suggests
303 extension-shear coupling within individual endocuticle
304 laminae; and further implies that ply-splitting occurred
305 via mode II fracture between macrofibers at high strain
306 [32, 33]. We hypothesize that intra-laminar extension-

307 shear coupling also yielded off-axis, in-plane resultant
308 forces as a function of lamina orientation angle. Mode III
309 shearing then occurred between laminae with opposing
310 in-plane resultant forces, causing the observed inter-ply
311 delamination. Tensile failure of the macrofiber laminae
312 would ultimately occur via mixed-mode I/II – i.e., trans-
313 verse tension/intra-laminar shear – fracture, due to an

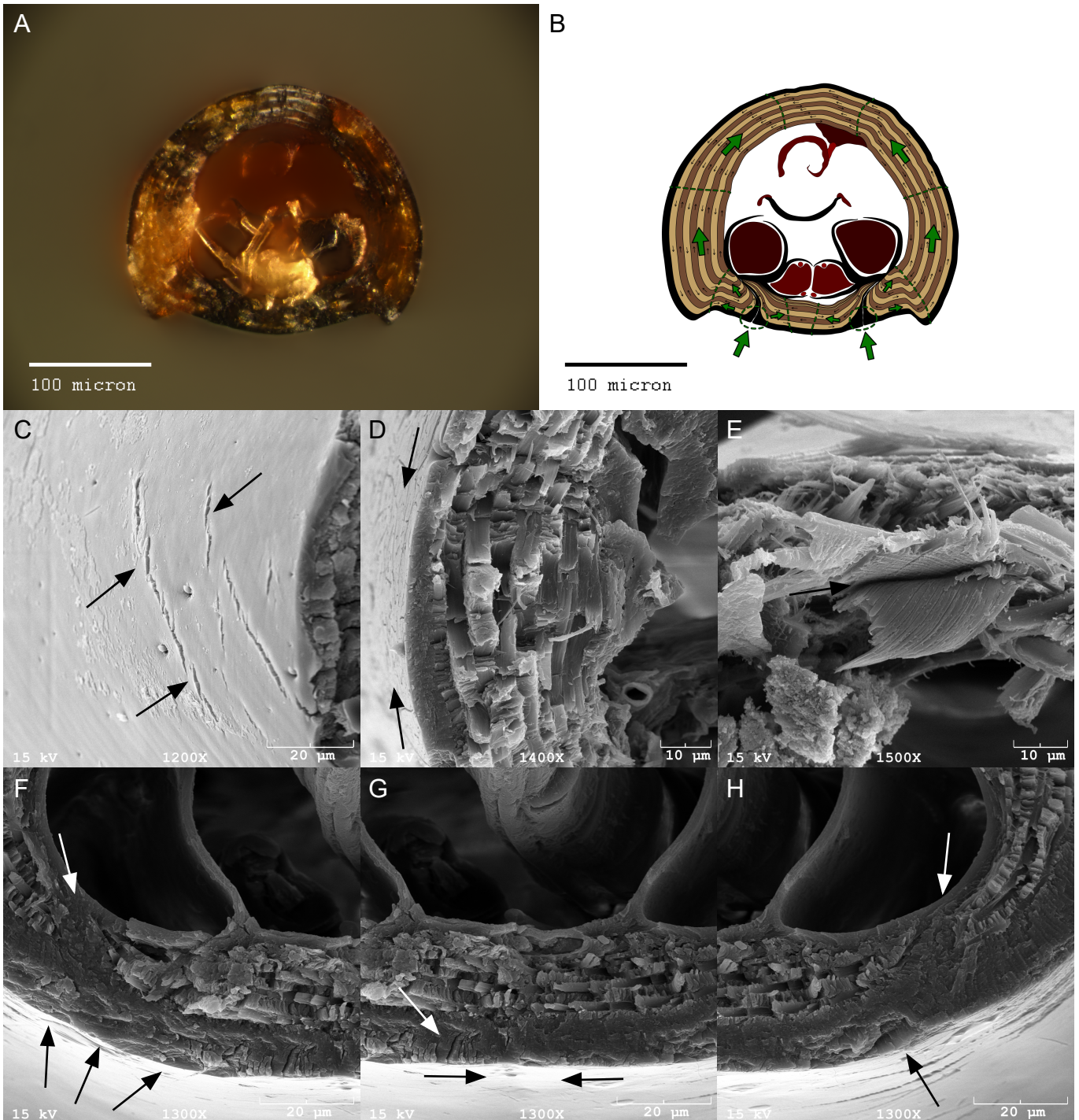


FIG. 6. Fractography of female *Curculio* rostrum. **a**, Light micrograph showing the fracture surface of tensile tested *Curculio carya* rostrum, displaying typical failure mode; illustrated in **(b)**: Small, black arrows indicate the winding direction of macrofiber laminae; green arrows and dotted lines indicate the direction of crack. Scanning electron micrographs highlight: **(c)** shear cusp formation; **(d)** tensile failure and off-axis macrofiber fiber-pulling; **(e)** interlaminar delamination; **(f-h)** crack formation near invaginated exocuticle; and **(g)** ventral crack-front coalescence and shear cusp formation.

increase in applied stress caused by ply-splitting in adjacent laminae [45].

At the meso-scale, most specimens fractured along a single plane across and between the occipital sulci, which

are cuticular invaginations that traverse the entire length of the rostrum [13, 17]. These sulci increase the volume fraction of exocuticle in the ventral part of the snout.

They contain large interfaces ideal for void nucleation

322 (Fig. 6). The exocuticle of the occipital sulci usually
 323 displayed shear cusps oriented outward from the center
 324 of the invagination, and continuing dorsolaterally and
 325 ventromedially. Ventrally, the cusps converged toward
 326 a prominent scarp where the crack fronts joined. This
 327 scarp was often obscured by delaminated endocuticular
 328 macrofibers in specimens with large cross-sectional areas
 329 of endocuticle,

330 The first layer of endocuticle usually fractured along
 331 the same plane as the exocuticle. Ventrally, the endocuti-
 332 cle laminae typically converged toward a scarp-like region
 333 characterized by severe delamination and numerous de-
 334 bonded macrofibers. Moreover, macrofibers aligned with
 335 the direction of crack propagation exhibited extensive
 336 ply-splitting with intermittent transverse shearing. In
 337 contrast, macrofibers oriented against the direction of
 338 crack propagation primarily displayed fracture by trans-
 339 verse shear along the plane of ply-splitting in adjacent
 340 laminae. Because the laminae form a cylinder, contralat-
 341 eral fibers in the same lamina display opposing fracture
 342 modes. The ventrolateral surfaces often exhibited ex-
 343 tensive inter-ply delamination and fiber de-bonding in
 344 scarp-like prominences. This is likely due to a combination
 345 of tensile failure and shearing along the dorsally-radiating
 346 crack front. Dorsally, the coalescent crack fronts often
 347 caused significant de-bonding and ply-splitting, followed
 348 by broom-like tensile failure. In some specimens, the con-
 349 tralateral crack fronts were out of plane and coalesced via
 350 transverse shear through a large dorsal section of cuticle.

351 Based on these failure patterns, we hypothesize that the
 352 exocuticle-rich occipital sulci are the most likely site for
 353 the initiation of void nucleation and catastrophic failure of
 354 the integrated rostral cuticle in cross section, as illustrated
 355 in Fig. 6. Structural failure would take place as cracks
 356 propagate through the endocuticle from these sutures, and
 357 ultimately penetrating the entire thickness of the laminate
 358 [13]. Although other, more complex failure modes have
 359 been observed, we posit that in live specimens this is the
 360 most likely mechanism of tensile failure because typical
 361 bending behavior generates tension *only* along the ventral
 362 surface of the rostrum.

363

V. CONCLUSIONS

364 The rostrum of *Curculio* is characterized by a discontin-
 365 uous composite profile. The cuticle is strongly differenti-
 366 ated in terms of relative layer thicknesses and orientation
 367 angles along an anterior-posterior gradient. These modifi-
 368 cations are sufficient to achieve a marked reduction in the
 369 effective membrane and flexural moduli of the cuticle –
 370 72% and 60%, respectively – in constitutive models based
 371 on CLPT, thereby accounting for the observed flexibil-
 372 ity of the rostral apex in live specimens. However, the
 373 reductions can only be realized with *both* modifications
 374 to the cuticle, which have a non-additive effect on cuticle
 375 elasticity. *Curculio* females require both modifications to
 376 function properly during oviposition.

377 Likewise, tensile and fatigue testing reveal a trade-off
 378 between stiffness and fracture resistance – measured by
 379 ultimate strain and toughness – mediated by the relative
 380 proportion of endocuticle in the laminate. The altered
 381 composite profile of the cuticle in the rostral apex makes
 382 the rostrum simultaneously more flexible and fracture
 383 resistant, permitting the structure to be flexed without
 384 exceeding the elastic limits of the cuticle.

385 This is to our knowledge the first time in arthropods
 386 that the composite profile of the cuticle has been related
 387 to a gradient in elasticity and tensile performance across
 388 a cuticular structure. Because these associations are
 389 independent of species membership, we posit that the
 390 behavior of the cuticle is consistent across the genus.
 391 Rostral flexibility is achieved exclusively in all *Curculio*
 392 species through a modified cuticle lay-up. This inference
 393 raises the intriguing possibility that a single ancestral shift
 394 in cuticle organization at the rostral apex – yielding higher
 395 flexibility and tensile strength – enabled the evolutionary
 396 “exploration” of a large morphospace region, promoting
 397 the high species-level diversity of this lineage.

398 Based on fractographic analysis of the test specimens,
 399 we infer that the exocuticle exhibits brittle fracture at
 400 a comparatively low strain, due to shearing between the
 401 endocuticle macrofibers to which it is anchored. These
 402 macrofibers fail at higher strain, mediated by mixed-
 403 mode shearing and tensile fracture within and between
 404 laminae. This outcome is consistent with behavior shown
 405 in previous studies, as well as theoretical consideration
 406 of cuticle microstructure in CLPT. The latter predicts
 407 extension shear-coupling ($A_{16}, A_{26} \neq 0$) for individual
 408 off-axis macrofiber laminae [32, 33].

409 Our results imply that fracture initiation occurs in the
 410 comparatively brittle exocuticle. The reduction in exocu-
 411 tile thickness in the rostral apex might serve to mitigate
 412 crack formation in rostral bending. Based on this pat-
 413 tern of fracture behavior, we identified the exocuticle-rich
 414 occipital suture as a common point of void nucleation
 415 and crack initiation. From an evolutionary perspective,
 416 these findings reveal an unexpected morphological source
 417 of constraint on rostral flexibility, raising the intriguing
 418 possibility that this system evolved primarily via nega-
 419 tive selection of fracture, rather than positive selection
 420 of flexibility. In particular, the cuticle is invaginated in
 421 precisely the portion of the snout that experiences the
 422 greatest degree of tension during antero-dorsal flexion.
 423 The doubly-thick exocuticle in the invagination thus cre-
 424 ates an unavoidable, brittle weak-point in an otherwise
 425 endocuticle-dominated rostral apex. This constraint – in
 426 conjunction with the minimization of exocuticle thickness
 427 in the rostral apex and the increased toughness derived
 428 from a thickened endocuticle – lead us to consider that
 429 avoidance of catastrophic structural failure has been a
 430 driving selective pressure in the evolution of the female
 431 *Curculio* rostrum.

VI. METHODS

436

432

433 Methods, including statements of data availability and
 434 any associated accession codes and references, are avail-
 435 able in the online version of this paper.

REFERENCES

- 437 [1] Jansen, M. A., Singh, S. S., Chawla, N., & Franz, N.
 438 M. A multilayer micromechanical model of the cuticle of
 439 *Curculio longinasus* Chittenden, 1927 (Coleoptera: Cur-
 440 culionidae). *J. Struct. Biol.* **195**: 2, 139–158, (2016).
- 441 [2] Vincent, J. F. V. & Wegst, U. G. K. Design and mechani-
 442 cal properties of insect cuticle. *Arthropod Struct. Dev.*
 443 **33**:3, 187–199, (2004).
- 444 [3] Hepburn, H. R. & Ball, A. On the structure and mechani-
 445 cal properties of beetle shells. *J. Mater. Sci.* **8**:5, 618–623,
 446 (1973).
- 447 [4] van de Kamp, T. & Greven, H. On the architecture of
 448 beetle elytra. *Entomol. Heute* **22**, 191–204, (2010).
- 449 [5] van de Kamp, T., Riedel, A. & Greven, H. Micromorphol-
 450 ogy of the elytral cuticle of beetles, with an emphasis on
 451 weevils (Coleoptera : Curculionoidea) *Arthropod Struct.*
 452 *Dev.* **45**:1, 14–22, (2016).
- 453 [6] Neville, A. C., Parry, D. A. & Woodhead-Galloway, J.
 454 The chitin crystallite in arthropod cuticle. *J. Cell Sci.*
 455 **21**:1, 73–82, (1976).
- 456 [7] Amini, S., Tadayon, M., Idapalapati, S., and Miserez, A.
 457 The role of quasi-plasticity in the extreme contact damage
 458 tolerance of the stomatopod dactyl club *Nat. Mater.* **14**:9,
 459 943–950, (2015).
- 460 [8] McCullough, E. L., Tobalske, B. W., and Emlen, D. J.
 461 Structural adaptations to diverse fighting styles in sexually
 462 selected weapons *Proc. Natl. Acad. Sci. USA* **111**:40,
 463 14484–14488, (2014).
- 464 [9] McCullough, E. L. Mechanical limits to maximum weapon
 465 size in a giant rhinoceros beetle *Proc. R. Soc. B* **281**,
 466 20140696, (2014).
- 467 [10] Dirks, J., Parle, E., and Taylor, D. Fatigue of insect
 468 cuticle *J. Exp. Biol.* **216**:10, 1924–1927, (2013).
- 469 [11] Dirks, J. and Taylor, D. Fracture toughness of locust
 470 cuticle *J. Exp. Biol.* **215**:9, 1502–1508, (2012).
- 471 [12] *International Code of Zoological Nomenclature* Fourth
 472 Edition. (The International Trust for Zoological Nomen-
 473 clature, London, 1999).
- 474 [13] Davis, S. R. *Morphology, phylogeny, and evolutionary
 475 development in the weevils (Insecta: Coleoptera: Cur-
 476 culionoidea)* (Ph.D. thesis, University of Kansas, 2014).
- 477 [14] Singh, S. S., Jansen, M. A., Franz, N. M., and Chawla,
 478 N. Microstructure and nanoindentation of the rostrum of
 479 *Curculio longinasus* Chittenden, 1927 (Coleoptera: Cur-
 480 culionidae) *Mater. Charact.* **118**, 206–211, (2016).
- 481 [15] Toju, H. and Sota, T. Imbalance of predator and prey
 482 armament: geographic clines in phenotypic interface and
 483 natural selection *Am. Nat.* **167**:1, 105–117, (2006).
- 484 [16] Gibson, L. P. Monograph of the genus *Curculio* in the
 485 New World (Coleoptera: Curculionidae). Part I. United
 486 States and Canada *Misc. Publ. Entomol. Soc. Am.* **6**,
 487 239–285, (1969).
- 488 [17] Dennell, R. The structure and function of the mouth-parts,
 489 rostrum and fore-gut of the weevil *Calandra granaria* L.
 490 *Phil. Trans. R. Soc. Lond. B* **231**:581, 247–291, (1942).
- 491 [18] Morimoto, K. and Kojima, H. Morphologic characters of
 492 the weevil head and phylogenetic implications (Coleoptera,
 493 Curculionoidea) *Esakia* **43**, 133–169, (2003).
- 494 [19] Ting, P. C. Feeding mechanisms of weevils, their function,
 495 and relationship to classification *Mon. Bull. Dep. Agric.*
 496 *State Calif.* **22**, 161–165, (1933).
- 497 [20] Ting, P. C. The mouth parts of the coleopterous group
 498 Rhynchophora *Microentomology* **1**, 93–114, (1936).
- 499 [21] Aguirre Uribe, L. A. *Biology of the immature stages of
 500 the pecan weevil Curculio caryaae (Horn) and oviposition
 501 habits of the adult weevil* (Ph.D. thesis, Texas A & M
 502 University, 1978).
- 503 [22] Moffett, M. Life in a nutshell *Natl. Geogr. Mag.* **176**,
 504 783–784, (1989).
- 505 [23] Longhai, L. et al. Microstructure and mechanical proper-
 506 ties of rostrum in Cyrtotrachelus longimanus (Coleoptera:
 507 Curculionidae) *Anim. Cells Syst.* **21**:3, 199–206, (2017).
- 508 [24] Matsumura, Y., Kovalev, A. E., and Gorb, S. N. Pen-
 509 tration mechanics of a beetle intromittent organ with
 510 bending stiffness gradient and a soft tip, *Sci. Adv.* **3**:12,
 511 eaao5469, (2017).
- 512 [25] Nikolov, S. et al. Robustness and optimal use of design
 513 principles of arthropod exoskeletons studied by ab initio
 514 based multiscale simulations. *J. Mech. Behav. Biomed.*
 515 *Mater.* **4**:2, 129–145, (2011).
- 516 [26] Nikolov, S. et al. Revealing the design principles of high-
 517 performance biological composites using Ab initio and
 518 multiscale simulations: The example of lobster cuticle.
 519 *Adv. Mater.* **22**:4, 519–526, (2010).
- 520 [27] Blackwell, J. and Weih, M. Structure of chitin-protein
 521 complexes: ovipositor of the ichneumon fly *Megarhyssa*.
 522 *J. Mol. Biol.* **137**:1, 49–60, (1980).
- 523 [28] Bouligand, Y. Twisted fibrous arrangements in biological
 524 materials and cholesteric mesophases. *Tissue Cell* **4**:2,
 525 189–217, (1972).
- 526 [29] Vincent, J. F. V. *Structural biomaterials* (Halsted Press,
 527 New York, 1982).
- 528 [30] Cheng, L., Wang, L., & Karlsson, A. M. Mechanics-based
 529 analysis of selected features of the exoskeletal microstruc-
 530 ture of *Popillia japonica*. *Mater. Res.* **24**:11, 3253–3267,
 531 (2009).
- 532 [31] Leopold, R. A., Newman, S. M., and Helgeson, G. A
 533 comparison of cuticle deposition during the pre-and poste-
 534 closion stages of the adult weevil, *Anthronomus grandis*
 535 BOHEMAN (Coleoptera: Curculionidae) *Int. J. Insect
 536 Morphol. and Embryol.* **21**:1, 37–62, (1992).
- 537 [32] Reddy, J. N. *Mechanics of laminated composite plates
 538 and shells: theory and analysis* (CRC Press, Philadelphia,
 539 2004).
- 540 [33] Jones, R. M. *Mechanics of composite materials* (CRC
 541 press, Philadelphia, 2014).

- 542 [34] Hughes, J. and Vogler, A. P. The phylogeny of acorn
543 weevils (genus *Curculio*) from mitochondrial and nuclear
544 DNA sequences: the problem of incomplete data *Mol.*
545 *Phylogenetic Evol.* **32:2**, 601–615, (2004).
- 546 [35] Bonal, R. et al. Diversity in insect seed parasite guilds at
547 large geographical scale: the roles of host specificity and
548 spatial distance *J. Biogeogr.* **43:8**, 1620–1630, (2016).
- 549 [36] Hughes, J. and Vogler, A. P. Ecomorphological adaptation
550 of acorn weevils to their oviposition site *Evolution* **58:9**,
551 1971–1983, (2004).
- 552 [37] Bonal, R., Espelta, J. M., and Vogler, A. P. Complex
553 selection on life-history traits and the maintenance of
554 variation in exaggerated rostrum length in acorn weevils
555 *Oecologia* **167:4**, 1053–1061, (2011).
- 556 [38] Klocke, D. & Schmitz, H. Water as a major modulator of
557 the mechanical properties of insect cuticle. *Acta Biomater.*
558 **7**, 2935–2942 (2011).
- 559 [39] Mihai, L. A. and Goriely, A. How to characterize a nonlin-
560 ear elastic material? A review on nonlinear constitutive
561 parameters in isotropic finite elasticity *Phil. Trans. R.*
562 *Soc. Lond. A* **473:2207**, 20170607, (2017).
- 563 [40] Münster, S. et al. Strain history dependence of the nonlin-
564 ear stress response of fibrin and collagen networks *Proc.*
565 *Natl. Acad. Sci. USA* **110:30**, 12197–12202, (2013).
- 566 [41] Felsenstein, J. Phylogenies and the comparative method
567 *Am. Nat.* **125:1**, 1–15, (1985).
- 568 [42] Revell, L. J. Phylogenetic signal and linear regression on
569 species data *Methods Ecol. Evol.* **1:4**, 319–329, (2010).
- 570 [43] Beament, J. W. L., Treherne, J. E., and Wigglesworth,
571 V. B. *Advances in insect physiology* Volume 4 (Academic
572 Press Inc., London, 1967).
- 573 [44] Sun, J. Y. et al. Differential constitutive equation of elytra
574 cuticle by nanoindentation *Adv. Mater. Res.*, **343**, 1133–
575 1139, (2012).
- 576 [45] Greenhalgh, E. *Failure analysis and fractography of poly-*
577 *mer composites* (CRC Press, Boca Raton, 2009).
- 597 in manuscript preparation. N.C. facilitated microscopy,
598 tensile and fatigue testing, and participated in manuscript
599 preparation. N.M.F. facilitated specimen acquisition and
600 imaging and participated in manuscript preparation.

ADDITIONAL INFORMATION

602 Supplementary information is available in the online ver-
603 sion of the paper. Reprints and permissions information
604 is available online at www.nature.com/reprints. Corre-
605 spondence and requests for materials should be addressed
606 to M.A.J.

COMPETING FINANCIAL INTERESTS

607 The authors declare no competing financial interests.

ACKNOWLEDGMENTS

578 The authors are grateful to Robert Anderson (CMNC),
579 Lourdes Chamorro (USNM), and Charlie O'Brien
580 (CWOB) for their assistance and provision of *Curculio*
581 specimens used in this study. The authors thank Salva-
582 tore Anzaldo, Andrew Johnston, Brian Reilly, Sangmi
583 Lee, and other Arizona State University Hasbrouck In-
584 sect Collection (ASUHIC) members for their assistance in
585 procuring, treating, and maintaining specimen loans upon
586 entry into the ASUHIC. The authors would also like to
587 thank David Lowry (ASU CLAS Bioimaging Center) for
588 his training and assistance with resin embedding, scanning
589 electron microscopy, and microtomography; and Salvatore
590 Anzaldo for his assistance with histological staining.

AUTHOR CONTRIBUTIONS

592 M.A.J. conducted sectioning and staining, microscopy
593 and imaging, tensile and fatigue testing, statistical anal-
594 ysis, and participated in manuscript preparation. J.W.
595 conducted tensile and fatigue testing and participated

609

METHODS

610

Specimen acquisition and taxon sampling

611 Specimens for use in tensile and fatigue testing came
 612 from the Hasbrouck Insect Collection at Arizona State
 613 University [ASUHIC]. This set of specimens was supple-
 614 mented with material housed in the following collections,
 615 using the codens of Arnett et al. [46]:

616 CMNC: Canadian Museum of Nature Collection, Ottawa,
 617 Ontario, Canada

618 USNM: National Museum of Natural History, Washington,
 619 D.C., USA

620 Cold fracture, semi-thin sectioning, and tensile testing
 621 were conducted on randomly chosen female specimens
 622 belonging to six *Curculio* species obtainable through field
 623 work in the southwestern United States and northwest-
 624 ern Mexico. Taxon sampling was targeted to represent
 625 a mixture of disparate radiations and sister taxa with
 626 a variety of rostral morphotypes in accordance with the
 627 phylogenetic hypotheses of Hughes et al. [34, 36] and
 628 Bonal et al. [35]. The six species of *Curculio* used herein
 629 are (in alphabetical sequence): *Curculio caryae* (Horn,
 630 1873), *Curculio humeralis* (Casey, 1897), *Curculio pro-*
boscideus Fabricius, 1775, *Curculio sulcatulus* (Casey,
 632 1897), *Curculio uniformis* (LeConte, 1857), and *Cur-*
culio victoriensis (Chittenden, 1904). Specimens were
 634 identified to taxonomic (species) concepts using [16] and
 635 other resources.

636

Histological sectioning

637 To illustrate the relative proportions of the cuticle re-
 638 gions in cross-section, serial semi-thin sectioning was con-
 639 ducted on exemplary female specimens of *Curculio humer-*
alis and *Curculio longinasus* Chittenden, 1927. Live spec-
 641 imens of both species were collected into 95% ethanol
 642 for preservation. A female specimen was selected; and
 643 the rostrum was separated from the head capsule with a
 644 fine-edged razor blade. The apical 1/4th of the rostrum
 645 was also removed and then discarded. The remaining
 646 portion of the rostrum and the head capsule were then
 647 embedded in EMbed812, as follows.

648 The cuticle was first immersed in acetone for 24 hours,
 649 and then transferred to a 2:1 mixture of acetone to epoxy
 650 resin. Samples remained at 21°C for 12 hours on a shaker
 651 table to prevent hardening. They were then transferred
 652 into a 1:1 mixture of acetone to resin, followed by a
 653 1:2 mixture (each for 12 hours and at 21°C on a shaker
 654 table), before finally being placed into a silicone mold
 655 with pure resin. The mold was placed into an oven heated
 656 to 38°C, and the resin was allowed to cure for 24 hours.
 657 The resulting blocks were machined to prepare the apical
 658 surface of each sample for microtomy.

659 A Leica Ultracut R Microtome and diamond knife were
 660 used to expose a cross-section (transverse plane) of the
 661 apical and basal portions of the rostrum and to remove ex-
 662 cess material. Semi-thin sections (0.5 µm thick) were kept
 663 and stained with toluidine-blue-borax for light microscopy
 664 and imaging.

665

Cold-fracture of specimens

666 Two pinned female specimens of each *Curculio* species
 667 were selected at random and retained for cold-fracturing
 668 of the rostrum. The heads of the specimens were removed
 669 and cleaned using a 95% ethanol solution and a thin paint-
 670 brush. Any muscles protruding from the occipital foramen
 671 were removed with a fine-edged razor blade. The anten-
 672 nae were removed directly using forceps to pull the scape
 673 (basal section of antenna) from the antennal insertion.
 674 Cleaned specimens were stored at -80°C for 24 hours,
 675 then fractured using forceps over a chilled aluminum block.
 676 To fracture each specimen, the head capsule and rostrum
 677 were each gripped firmly in a pair of forceps. The forceps
 678 were then sharply rotated to fracture the base of the snout
 679 via dorsal flexion. The rostrum was fractured a second
 680 time, after separation from the head capsule, using the
 681 same procedure. The segmented specimens were then
 682 placed into individual glass vials to protect the fracture
 683 surfaces from contamination prior to microscopy.

684

Tensile and fatigue testing

685 *Force-controlled loading to failure.* Five female speci-
 686 mens of each *Curculio* species were randomly allocated
 687 for use in tensile testing. The head of each specimen was
 688 removed, cleaned, and prepared as described above in the
 689 cold-fracture protocol. To avoid destroying the delicate,
 690 brittle specimens when gripping the ends of each head, a
 691 method was devised to create solid handles that could be
 692 clamped tightly into grips without risk of damage to the
 693 cuticle.

694 For each head, four 1 cm² strips of gaffer tape were
 695 cut; these were used as gripping and mounting points
 696 for the specimen. A strip of tape would be laid flat,
 697 with a large drop of cyanoacrylate glue placed upon the
 698 upturned surface. The curved portion of the snout was
 699 then placed into the drop, such that the straight portion
 700 of the rostrum was aligned perpendicular to the edge
 701 of the strip. Hardening of the cyanoacrylate effectively
 702 embedded the curved portion of the snout in a solid
 703 mass, isolating a straight section of the snout – from the
 704 base to a point distad of the apex of the scrobe – for
 705 testing. A second strip of tape was fixed over this mass
 706 with an additional layer of cyanoacrylate to provide a
 707 dorsal gripping surface for the mass. A small mark was
 708 made to indicate the extent of the head inside the mass.
 709 This embedding procedure was repeated for the head

710 capsule, resulting in a finished specimen with anterior 765
 711 and posterior handles for testing.

712 Prior to testing, each specimen was placed in de-ionized 766
 713 water for 24 hours to allow full saturation of the cuticle, 767
 714 simulating the condition of live tissue [38]. Once removed 768
 715 for testing, the specimen was gripped using the cyanoacry- 769
 716 late handles at the marked locations immediately beyond 770
 717 the anterior margin of the rostrum and the posterior mar- 771
 718 gin of the head capsule. The exposed section of the snout 772
 719 was coated in petroleum jelly using a cotton swab to 773
 720 prevent loss of moisture and stiffening of the specimen 774
 721 during the test. Specimens were loaded in a Tryton 250 775
 722 Microforce Testing System equipped with a 5N load cell 776
 723 and mechanical clamp grip. All specimens were subjected 777
 724 to force-controlled uniaxial tension at a rate of $1.0 \text{ gf} \cdot \text{s}^{-1}$ 778
 725 until failure, with a sampling interval of 0.1 s. Engineer- 779
 726 ing stresses ($\sigma_0 = F/A_0$) and strains ($\epsilon_0 = \Delta l/l_0$) were 780
 727 reported only for specimens that did not fracture due to 781
 728 strain accumulation at the interface between the rostrum 782
 729 and the cyanoacrylate handles.

730 *Displacement-controlled cyclic loading.* To confirm 783
 731 that repeated, complete extension of a strongly curved 784
 732 rostrum would not result in fracture of the cuticle, a 785
 733 representative female specimen of *Curculio caryae* was 786
 734 allocated for fatigue testing. The head capsule of the 787
 735 specimen was fixed to a push-pin using cyanoacrylate 788
 736 glue. This served as a pedestal and gripping location 789
 737 for the posterior portion of the specimen. The apex of 790
 738 the rostrum was fixed to a strip of ripstop nylon fabric 791
 739 equal in length to the head, using cyanoacrylate glue. As 792
 740 with tensile testing, the specimen was placed in de-ionized 793
 741 water for 24 hours, then coated in petroleum jelly using 794
 742 a cotton swab immediately prior to load cycling.

743 The end of the fabric was gripped and used to elon- 795
 744 gate the rostrum in tension by pulling on the fabric, thus 796
 745 isolating the effect of tension on the fatigue life of the 797
 746 rostral cuticle. In this way, the rostrum would return to 798
 747 its original configuration in a spring-like manner, as in 799
 748 living specimens, rather than being forced to return to the 800
 749 initial position. The rostrum was aligned such that com- 801
 750 plete elongation of the curved section would take place in 802
 751 tension, with minimal off-axis deflection of the un-curved 803
 752 section. The specimen was subjected to displacement- 804
 753 controlled loading sufficient to fully extend the rostrum 805
 754 and generate a load stress of 1 N, or approximately 20% of 806
 755 the tensile strength of the species average. Load cycling 807
 756 took place at a rate of 0.33Hz, and was continued for 14 808
 757 days – i.e., 400,000 cycles – until the tensile stress in the 809
 758 sample approached an asymptotic minimum.

759 Once the test was concluded, the specimen was placed in 810
 760 a 50% ethanol solution for 24 hours to clean the petroleum 811
 761 jelly from the rostrum. The specimen was examined for 812
 762 surface fractures and micro-tears, then subjected to tensile 813
 763 testing via the same protocol as the other specimens to 814
 764 assess whether the cuticle had begun to fatigue.

Specimen imaging and microscopy

766 The fracture surfaces of cold-fractured specimens were 767
 768 examined using scanning electron microscopy to charac- 769
 769 terize the composite profile and microstructure of the 770
 771 rostrum. Fracture behavior of tensile testing specimens 772
 772 was assessed using both light microscopy and SEM to 773
 773 image the fracture surfaces of the specimens in transverse 774
 774 view. Electron microscopy was conducted using a JEOL 775
 775 JSM6300 scanning electron microscope. Light microscopy 776
 776 was conducted using a Leica M205 C stereomicroscope 777
 777 and attached computer running the software Leica Appli- 778
 778 cation Suite (LAS); as well as a Visionary Digital Passport 779
 779 II system using a Canon EOS Mark 5D II camera outfit- 780
 780 ted with interchangeable macro lenses. Specimen length, 781
 781 layer thicknesses, macrofiber orientation angles, and cross- 782
 782 sectional areas were measured in the LAS and in Adobe 783
 783 Illustrator, using pixel-wise measurements multiplied by 784
 784 a scaling factor for the image.

Constitutive modeling of the cuticle

784 *General approach.* The effective uni-axial membrane 785
 785 and transverse flexural elastic moduli of idealized cuticle 786
 786 organizations, representing both the rostral apex and head 787
 787 capsule, were estimated using Classical Laminate Plate 788
 788 Theory (CLPT). For general information on this approach 789
 789 see [32, 33]. The composite profiles of both types of cuticle 790
 790 were idealized using the layer thicknesses and stacking se- 791
 791 quences observed in *Curculio longinasus*. This particular 792
 792 species was chosen because we derived the effective elastic 793
 793 constants of the individual components of the cuticle in 794
 794 previous work [1, 14]. In addition, *Curculio longinasus* 795
 795 exhibits a profile that is typical and representative for the 796
 796 genus *Curculio*, based on examination of the six species 797
 797 used for tensile testing.

798 For *Curculio longinasus* the total thickness of the 800
 799 cuticle in the head and rostrum is roughly 50 μm , 801
 800 as in most specimens of the other examined species. 802
 801 In the head capsule, the exocuticle occupies between 803
 802 30-50% of the through-thickness of the laminate, with 804
 803 the remaining thickness nearly evenly divided between 804
 804 12 layers of endocuticle. We use the maximum (50% 805
 805 of through-thickness, or 25 μm) for the model, since 806
 806 the cuticle appears to deviate from this value only in 807
 807 regions with sulci (grooves), pores, and other scattered 808
 808 features of the surface sculpture. The macrofiber lami- 809
 809 nae of the endocuticle were assigned a stacking sequence of 810
 810 $0^\circ, 90^\circ, 30^\circ, -60^\circ, 60^\circ, -30^\circ, 90^\circ, 0^\circ, -60^\circ, 30^\circ, -30^\circ, 60^\circ;$ 811
 811 thereby representing pairs of orthogonal plies stacked at 812
 812 a constant rotation angle of 30° , in approximation of the 813
 813 living tissue.

814 In the rostral apex, the exocuticle is reduced to a thin 815
 815 shell approximately 5 μm in thickness, or 10% of the 816
 816 total cuticle thickness. The endocuticle displays a more 817
 817 complex pattern of layer thicknesses in the rostral apex 818
 818 than in the head capsule. Each of the eight outermost

⁸¹⁹ layers are of nearly equal thickness to the exocuticle (5
⁸²⁰ μm), whereas the four innermost layers have a combined
⁸²¹ thickness equal to that of the exocuticle or to a single layer
⁸²² of outer endocuticle ($h_{\text{outer}} = 5 \mu\text{m}$, $h_{\text{inner}} = 1.25 \mu\text{m}$).
⁸²³ The stacking sequence with respect to the longitudinal
⁸²⁴ axis of the rostrum forms an antisymmetric angle-ply
⁸²⁵ laminate of $\pm 45^\circ$.

⁸²⁶ To assess the individual contributions of layer thickness
⁸²⁷ and stacking angle sequence to cuticle flexibility in the
⁸²⁸ rostral apex, two hypothetical cuticle lay-ups were mod-
⁸²⁹ eled – each with only one of the modifications present in
⁸³⁰ the cuticle of the rostral apex. The first of these models
⁸³¹ has the layer thicknesses of the rostral apex, but fiber
⁸³² orientations of the head capsule; whereas the second has
⁸³³ the fiber orientations of the rostral apex, but the layer
⁸³⁴ thicknesses of the head capsule.

⁸³⁵ Because these laminates are not symmetric, each has
⁸³⁶ a bending-extension coupling matrix $[B]$ populated with
⁸³⁷ non-zero terms; thus complicating the calculation of effec-
⁸³⁸ tive in-plane elastic moduli. To circumvent this difficulty
⁸³⁹ and enable meaningful comparisons between each lam-
⁸⁴⁰ inate, all of the lay-ups are reflected about their inner
⁸⁴¹ surface. This effectively doubles their thickness while pro-
⁸⁴² ducing a balanced, symmetric laminate with no coupling
⁸⁴³ between bending and extension (i.e., $[B] = 0_{3,3}$). Estima-
⁸⁴⁴ tion of in-plane elastic constants from the extension($[A]$)
⁸⁴⁵ and bending ($[D]$) matrices is described in detail below.
⁸⁴⁶ The program Matlab R2018b was used to numerically
⁸⁴⁷ evaluate the final values of the effective elastic constants
⁸⁴⁸ [47].

⁸⁴⁹ *Classical Laminate Plate Theory.* We begin by calcu-
⁸⁵⁰ lating the 2D reduced stiffness matrix for each part of the
⁸⁵¹ cuticle. For orthotropic materials with the principal axes
⁸⁵² parallel to the ply edges, the reduced stiffness matrix is
⁸⁵³ defined as follows:

$$[Q] = \begin{bmatrix} Q_{11} & Q_{12} & 0 \\ Q_{21} & Q_{22} & 0 \\ 0 & 0 & Q_{66} \end{bmatrix}, \quad (1)$$

⁸⁵⁴ where:

$$\begin{aligned} Q_{11} &= \frac{E_1}{1 - \nu_{12}\nu_{21}}, \\ Q_{12} &= \frac{E_1\nu_{21}}{1 - \nu_{12}\nu_{21}} = Q_{21}, \\ Q_{21} &= \frac{E_2\nu_{12}}{1 - \nu_{12}\nu_{21}} = Q_{12}, \\ Q_{22} &= \frac{E_2}{1 - \nu_{12}\nu_{21}}, \\ Q_{66} &= G_{12}. \end{aligned} \quad (2)$$

⁸⁵⁵ For each layer k , the reduced stiffness matrix is trans-
⁸⁵⁶ formed to account for the layer orientation angle θ within
⁸⁵⁷ the laminate coordinate system, yielding a reduced trans-
⁸⁵⁸ formed stiffness matrix according to:

$$[\bar{Q}] = [T]^{-1}[Q][T]^{-T}, \quad (3)$$

⁸⁵⁹ where the transformation matrix $[T]$ is defined as:

$$[T] = \begin{bmatrix} \cos^2 \theta & \sin^2 \theta & 2 \cos \theta \sin \theta \\ \sin^2 \theta & \cos^2 \theta & -2 \cos \theta \sin \theta \\ -\cos \theta \sin \theta & \cos \theta \sin \theta & \cos^2 \theta - \sin^2 \theta \end{bmatrix}. \quad (4)$$

⁸⁶⁰ Using the lay-ups specified for each type of cuticle
⁸⁶¹ described above, we calculate the extensional stiffness
⁸⁶² matrix $[A]$, bending stiffness matrix $[D]$, and bending-
⁸⁶³ extension coupling matrix $[B]$ for each laminate consisting
⁸⁶⁴ of n layers at a distance z from the laminate mid-plane.
⁸⁶⁵ The elements of these matrices can be identified according
⁸⁶⁶ to:

$$\begin{aligned} A_{ij} &= \sum_{k=1}^n (\bar{Q}_{ij})_k (z_k - z_{k-1}), \\ B_{ij} &= \frac{1}{2} \sum_{k=1}^n (\bar{Q}_{ij})_k (z_k^2 - z_{k-1}^2), \\ D_{ij} &= \frac{1}{3} \sum_{k=1}^n (\bar{Q}_{ij})_k (z_k^3 - z_{k-1}^3). \end{aligned} \quad (5)$$

⁸⁶⁷ These stiffness matrices respectively relate vectors of
⁸⁶⁸ resultant forces $\{N\}$ and bending moments $\{M\}$ to mid-
⁸⁶⁹ surface strains and curvatures $\{\epsilon^\circ\}$ and $\{\kappa\}$ in the lami-
⁸⁷⁰ nate, according to the following relationship:

$$\begin{Bmatrix} \{N\} \\ \{M\} \end{Bmatrix} = \begin{bmatrix} [A] & [B] \\ [B] & [D] \end{bmatrix} \begin{Bmatrix} \{\epsilon^\circ\} \\ \{\kappa\} \end{Bmatrix}. \quad (6)$$

⁸⁷¹ For symmetric laminates, $[B] = 0_{3,3}$, and therefore:

$$\begin{aligned} \{N\} &= [A]\{\epsilon^\circ\}, \\ \{M\} &= [D]\{\kappa\}, \end{aligned} \quad (7)$$

⁸⁷² or, in expanded form:

$$\begin{aligned} \begin{Bmatrix} N_{xx} \\ N_{yy} \\ N_{xy} \end{Bmatrix} &= \begin{bmatrix} A_{11} & A_{12} & A_{16} \\ A_{21} & A_{22} & A_{26} \\ A_{61} & A_{62} & A_{66} \end{bmatrix} \begin{Bmatrix} \epsilon_{xx}^\circ \\ \epsilon_{yy}^\circ \\ \gamma_{xy}^\circ \end{Bmatrix}, \\ \begin{Bmatrix} M_{xx} \\ M_{yy} \\ M_{xy} \end{Bmatrix} &= \begin{bmatrix} D_{11} & D_{12} & D_{16} \\ D_{21} & D_{22} & D_{26} \\ D_{61} & D_{62} & D_{66} \end{bmatrix} \begin{Bmatrix} \kappa_{xx} \\ \kappa_{yy} \\ \kappa_{xy} \end{Bmatrix}. \end{aligned} \quad (8)$$

⁸⁷³ If we make the simplifying assumptions [32, 33] that
⁸⁷⁴ (1) the laminate experiences pure axial loading and trans-
⁸⁷⁵ verse bending (i.e., $N_{yy} = N_{xy} = 0$ and $M_{yy} = M_{xy} = 0$,
⁸⁷⁶ respectively), and (2) the laminate is a beam of suffi-
⁸⁷⁷ ciently high aspect ratio to minimize the Poisson effect
⁸⁷⁸ and anisotropic shear coupling (i.e., below we effectively

879 let $A_{12}^* = A_{16}^* = 0$ and $D_{12}^* = D_{16}^* = 0$), then we can
 880 calculate the in-plane effective flexural and axial Young's
 881 moduli of the laminate along the x-axis.

882 For axial Young's modulus of the laminate, we first
 883 define the average membrane stresses in the laminate as:

$$\{\bar{\sigma}^m\} = \frac{\{N\}}{z_1 - z_n}. \quad (9)$$

884 By substitution in Eq. 7, we obtain:

$$\begin{Bmatrix} \bar{\sigma}_{xx}^m \\ \bar{\sigma}_{yy}^m \\ \bar{\tau}_{xy}^m \end{Bmatrix} = \frac{1}{(z_1 - z_n)} \begin{bmatrix} A_{11} & A_{12} & A_{16} \\ A_{21} & A_{22} & A_{26} \\ A_{61} & A_{62} & A_{66} \end{bmatrix} \begin{Bmatrix} \epsilon_{xx}^m \\ \epsilon_{yy}^m \\ \gamma_{xy}^m \end{Bmatrix}, \quad (10)$$

885 and, by inverting this equation (let $A^* = A^{-1}$) and
 886 substituting $A_{12}^* = A_{16}^* = 0$ based on the assumptions
 887 above, we infer:

$$\epsilon_{xx}^m = (z_1 - z_n) A_{11}^* \bar{\sigma}_{xx}^m. \quad (11)$$

888 We therefore define Young's modulus for effective axial
 889 elasticity as:

$$E_{xx}^m = \frac{\bar{\sigma}_{xx}^m}{\epsilon_{xx}^m} = \frac{1}{(z_1 - z_k) A_{11}^*}. \quad (12)$$

890 To find the transverse flexural Young's modulus of the
 891 laminate, we first specify the moment-curvature relation
 892 of an Euler-Bernoulli beam:

$$M = EI\kappa. \quad (13)$$

893 Along the x-axis, the second moment of area for a
 894 rectangular cross-section is:

$$I_{yy} = \frac{b(z_1 - z_n)^3}{12}. \quad (14)$$

895 Given the assumption that $M_{yy} = M_{xy} = 0$, the mo-
 896 ment along the x-axis is related to the moment of the
 897 beam by:

$$M = M_{xx}b. \quad (15)$$

898 Thus, given the assumption that $D_{12}^* = D_{16}^* = 0$,
 899 Young's modulus for the effective transverse flexural elas-
 900 ticity of the laminate can be found by making Eq. 13
 901 specific to transverse flexure of the x-axis and rearranging
 902 the terms:

$$E_{xx}^f = \frac{12M_{xx}}{(z_1 - z_n)^3 \kappa_{xx}}. \quad (16)$$

903 From inversion of Eq. 7 (let $D^* = D^{-1}$), this reduces
 904 to:

$$E_{xx}^f = \frac{12}{(z_1 - z_n)^3 D_{11}^*}. \quad (17)$$

Statistical analysis

906 *Model selection and fitting.* In order to explore the
 907 relationships between the composite structure and me-
 908 chanical properties of the cuticle, we fit phylogenetic
 909 linear mixed-effects models (PGLMM) to the tensile
 910 testing data using maximum likelihood estimation [48–
 911 51]. Raw data was processed using a custom script in
 912 Python version 3.5.2 [52]. Model exploration and fitting
 913 was conducted in R version 3.5.1 (2018-07-02) --
 914 ‘Feather Spray’, using the ‘nlme’ and ‘ape’ pack-
 915 ages [53–55]. Response variables and covariates were
 916 natural-log transformed, as needed, to ensure that the
 917 normalized model residuals were normally distributed
 918 [R:shapiro.test] and homoscedastic [R:levene.test],
 919 using numerical and graphical analysis. In order to con-
 920 trol for phylogenetic non-independence in the data, we
 921 included the species of each specimen as a random ef-
 922 fect in all models. We also allowed for correlation in
 923 the error term of the models, as specified by a variance-
 924 covariance matrix generated from a Brownian motion
 925 model of trait evolution [R:‘ape’:corBrownian] along a
 926 phylogeny [54, 56].

927 The preferred phylogeny for select North American *Cur-*
928 culio species is that of Bonal et al. [35]. This phylogeny
 929 was generated using Maximum-Likelihood methods; it is
 930 untrammatic yet has uniform internal branch lengths. The
 931 preferred tree was pruned to include only those species
 932 used in tensile testing, with a polytomy at each species'
 933 root node to represent the individual specimens examined
 934 for that species. Because the branch lengths of the tree
 935 were not specified, all branch lengths were set equal to 1.
 936 Underestimation of branch lengths causes overestimation
 937 of phylogenetic signal [56–58]. We were unable to detect
 938 statistically significant phylogenetic signal for any of our
 939 models. For this reason we consider our study's principal
 940 findings to be unaffected by branch length underestima-
 941 tion. However, because of the relatively poor taxonomic
 942 resolution afforded by a sample of five species, we are
 943 unable to conclude whether significant phylogenetic signal
 944 exists in the traits examined herein.

945 Other models of trait evolution were considered dur-
 946 ing model exploration; including Ornstein-Uhlenbeck
 947 [R:‘ape’:corMartins] and variable rate (AC/DC) mod-
 948 els [R:‘ape’:corBlomberg] [54, 56]. These models were
 949 chosen to compare among competing hypotheses of trait
 950 evolution, namely stabilizing selection and variable-rate
 951 evolution, respectively. We additionally tested a Brownian
 952 motion model of trait evolution, corresponding to varia-
 953 tion constrained by clade membership (i.e., sister taxa are
 954 more similar to each other than to an out-group). How-
 955 ever, neither of the former produced a significantly better
 956 fit to the data than the Brownian motion model for any
 957 comparison, as measured by likelihood score and residual
 958 variance; viz. R_σ^2 , and $R_{\beta^*}^2$ [R:‘r2glmm’:r2beta]. R_σ^2
 959 is the proportion of generalized variance explained by
 960 fixed effects. This measure is generally used for compar-
 961 ison of covariance structures [59–61]. $R_{\beta^*}^2$ measures the

multivariate association between the outcome and the likelihood-ratio tests and $R^2_{\beta^*}$ -difference tests between fixed effects within a given correlation structure, and is each of the three models. Only the cross-sectional area generally used to compare fixed effects [59–61]. Using of endocuticle produced a significant fixed effect. We therefore elected to make the model more parsimonious phylogenetic signal in the residual variance of each model; by removing cross-sectional area of exocuticle as a fixed taking into account two measures of spatial autocorrelation (Abouheif's \bar{C} and Moran's I), and two measures of the ratio of exocuticle to endocuticle in cross-section as a phylogenetic signal (Pagel's λ and Blomberg's κ). The final model generated for our first aim featured a fixed effect, with ultimate tensile strength as the response variable.

In all models, we tested whether the inclusion of phylogenetic correlation in the model error produced significantly better model fit, using a likelihood-ratio test [R: 'lmtree': lrtest] and R^2_{σ} -difference test [R: 'r2glmm': r2beta(method='sgv')] between the fully-specified model and a model lacking the phylogenetic effect [61, 63]. Models that incorporated covariance due to Brownian motion consistently produced higher likelihood scores and fit to the data. However, no model exhibited statistically significant phylogenetic signal in any of the variables. Our findings imply that *residual variance* in the examined traits does not exhibit significant rate-variation or stabilizing selection in the amount or direction of residual variance between groups; rather, variation within and between clades is distributed randomly by clade, with limited phylogenetic dependence. Once models were fitted to the data, T- and F-statistics were calculated to determine whether each cofactor was significantly different from zero.

Hypothesis testing. Our objectives for hypothesis testing using the PGLMMs were threefold: (1) to assess whether the altered ratio of exocuticle to endocuticle in the rostral apex has an effect on the tensile strength of the rostrum; (2) to test whether a trade-off exists between specimen stiffness and resistance to fracture; and (3) to examine whether rostrum length and flexibility are correlated.

To test the relationship between relative layer thicknesses and tensile strength, we fitted a fully-specified model with the cross-sectional area of exocuticle and endocuticle at the site of fracture as fixed effects, including an interaction term, and with the maximum tensile force sustained prior to fracture as a response variable. This model was then compared to models with only cross-sectional area of either endocuticle or exocuticle, but not both, as the sole fixed effect in the model. We then tested whether one or both regions were significantly correlated to the maximum force sustained in tension, using request.

For our second aim we examined the relationship between specimen stiffness and resistance to fracture. Specimen stiffness was characterized using a low strain elastic modulus – averaged across the first 33% of the stress-strain curve – and the secant modulus at failure. Resistance to fracture was quantified in terms of ultimate strain and work of fracture, measured as area under the stress-strain curve. Four models were fitted, two of which had ultimate strain as the response variable, and two with work of fracture as response variable. Each model then used one of the different measures of specimen stiffness as a fixed effect.

Finally, for the third aim we explored whether a size-effect might exist in the *Curculio* rostrum; and specifically if longer and typically more curved rostra were more flexible than shorter, straighter rostra. We generated two models; the low strain and secant elastic moduli individually served as response variables, with specimen length as the fixed effect in both.

Code availability

R, Python, and Matlab scripts used to manipulate and analyze the raw data (as well as their outputs), produce figures, and estimate effective elastic constants are available from the corresponding author upon request.

Data availability

Stress-strain curves for all tensile and fatigue-tested specimens are provided as PDFs (Supplement 1). Diagnostic plots for all PGLMMs are provided as PDFs (Supplement 2). PGLMM terms and output are provided in a PDF (Supplement 3). Raw and processed data will be provided by the corresponding author upon reasonable request.

1049

REFERENCES

- 1050 [46] Arnett Jr., R. H., Samuelson, G. A., and Nishida G. M. *The Insect and Spider Collections of the World*, 2nd Edition. Fauna and Flora Handbook No. 11. (Sandhill Crane Press, Gainesville, 1993).
- 1051 [47] The MathWorks, Inc., *MATLAB and Statistics Toolbox* (Natick, Mass., Release R2018b, 2018).
- 1056 [48] Galecki, A. and Burzykowski, T. *Linear Mixed-Effects Models Using R. A Step-by-Step Approach* (Springer, New York, 2013).
- 1057 [49] Hadfield, J. D. and Nakagawa, S. General quantitative genetic methods for comparative biology: phylogenies, taxonomies and multi-trait models for continuous and categorical characters *J. Evol. Biol.* **23**:3, 494–508, (2010).

- 1063 [50] Housworth, E. A., Martins, E. P., and Lynch, M. The Phylogenetic Mixed Model. *Am. Nat.* **163**:1, 84–96, (2004). 1082
- 1064 [51] Stone, G. N., Sean, N., and Felsenstein, J. Controlling for non-independence in comparative analysis of patterns across populations within species. *Philos. Trans. Royal Soc. B* **366**:1569, 1410–1424, (2011). 1083
- 1065 [52] Python Core Team. *Python: A dynamic, open source programming language* (Python Software Foundation, Version 3.5.2, 2018). 1088
- 1066 [53] R Development Core Team *R: A Language and Environment for Statistical Computing* (R Foundation for Statistical Computing, Vienna, Version 3.5.1, 2008). 1091
- 1067 [54] Paradis, E. and Schliep, K. ape 5.0: an environment for modern phylogenetics and evolutionary analyses in R. *Bioinformatics* **5**:0, (2018). 1094
- 1068 [55] Pinheiro, J. et al. nlme: Linear and Nonlinear Mixed Effects Models **R package version 3.1-137**, (2018). 1097
- 1069 [56] Münkemüller, T. et al. How to measure and test phylogenetic signal. *Methods Ecol. Evol.* **3**:4, 743–756, (2012). 1099
- 1070 [57] Stone, E. A. Why the phylogenetic regression appears robust to tree misspecification. *Syst. Biol.* **60**:3, 245–260, (2011). 1084
- 1071 [58] Molina-Venegas, R. and Rodríguez, M. Á. Revisiting phylogenetic signal; strong or negligible impacts of polytomies and branch length information? *BMC Evol. Biol.* **17**:1, 1–53, (2017). 1087
- 1072 [59] Nakagawa, S. and Schielzeth, H. A general and simple method for obtaining R² from generalized linear mixed-effects models. *Methods Ecol. Evol.* **4**:2, 133–142, (2013). 1090
- 1073 [60] Jaeger, B. C., Edwards, L. J., Das, K., and Sen, P. K. An R² statistic for fixed effects in the generalized linear mixed model. *J. Appl. Stat.* **44**:6, 1086–1105, (2016). 1093
- 1074 [61] Jaeger, B. Computes R Squared for Mixed (Multilevel) Models **Version 0.1.2** (2017). 1096
- 1075 [62] Liam, J. R. phytools: An R package for phylogenetic comparative biology (and other things). *Methods Ecol. and Evol.* **3**, 217–223, (2012). 1098
- 1076 [63] Zeileis, A. and Hothorn, T. Diagnostic Checking in Regression Relationships *R News* **2**:3, 7–10, (2002). 1101